Original Article

MOLECULAR METABOLISM

BBSome ablation in SF1 neurons causes obesity without comorbidities

Mohamed Rouabhi [1,9], Deng-Fu Guo [1,2,9], Donald A. Morgan [1,2], Zhiyong Zhu [2,3], Miguel López [4], Leonid Zingman [2,3,5,6], Justin L. Grobe [1,5,6,7,8], Kamal Rahmouni [1,2,3,5,6,7,*]

ABSTRACT

Objectives: The hypothalamic ventromedial nucleus (VMH) plays a major role in metabolic control, but the molecular mechanisms involved remain poorly defined. We analyzed the relevance of the BBSome, a protein complex composed of 8 Bardet–Biedl syndrome (BBS) proteins including BBS1, in VMH steroidogenic factor 1 (SF1) neurons for the control of energy homeostasis and related physiological processes.
Methods: We generated mice bearing selective BBSome disruption, through *Bbs1* gene deletion, in SF1 neurons ($SF1^{Cre}/Bbs1^{fl/fl}$). We analyzed the consequence on body weight, glucose homeostasis, and cardiovascular autonomic function of BBSome loss in SF1 neurons.
Results: $SF1^{Cre}/Bbs1^{fl/fl}$ mice had increased body weight and adiposity under normal chow conditions. Food intake, energy absorption, and digestive efficiency were not altered by *Bbs1* gene deletion in SF1 neurons. $SF1^{Cre}/Bbs1^{fl/fl}$ mice exhibited lower energy expenditure, particularly during the dark cycle. Consistent with this finding, $SF1^{Cre}/Bbs1^{fl/fl}$ mice displayed reduced sympathetic nerve traffic and expression of markers of thermogenesis in brown adipose tissue. $SF1^{Cre}/Bbs1^{fl/fl}$ mice also had lower sympathetic nerve activity to subcutaneous white adipose tissue that was associated with a protein expression profile that promotes lipid accumulation. Notably, despite obesity and hyperinsulinemia, $SF1^{Cre}/Bbs1^{fl/fl}$ mice did not exhibit significant changes in glucose metabolism, insulin sensitivity, blood pressure, and baroreflex sensitivity.
Conclusions: Our findings demonstrate that the SF1 neuron BBSome is necessary for the regulation of energy homeostasis through modulation of the activity of the sympathetic nervous system and that the SF1 neuron BBSome is required for the development of obesity-related comorbidities.

Keywords Bardet–biedl syndrome proteins; Hypothalamus; Obesity; Hypertension; Insulin resistance

1. INTRODUCTION

The high prevalence of obesity is associated with increased mortality because of various comorbidities evoked by an increase in adiposity. Type II diabetes and cardiovascular disease are major medical conditions commonly linked to alterations in the homeostatic pathways that regulate energy homeostasis [1,2]. As a master regulator of energy balance, the brain integrates peripheral signals and, in turn, modulates feeding behavior and the activity of the autonomic nervous system. The hypothalamus acts as the main hub that receives and integrates peripheral signals [3].

The importance of the hypothalamic ventromedial nucleus (VMH) in metabolic control is well established [4–6]. Through the sympathetic nervous system (SNS), the VMH is involved in the regulation of thermogenic activity of brown adipose tissue (BAT) and the modulation of lipid metabolism of white adipose tissue (WAT) [6–8]. The VMH is also involved in the control of glucose homeostasis as altering the activity of VMH neurons affect insulin sensitivity and blood glucose levels [6,7,9,10]. The VMH also projects to many other tissues that regulate physiological processes, including blood pressure [11]. Within the VMH, neurons expressing steroidogenic factor 1 (SF1) have emerged as key mediators of metabolic control [12]. SF1 neurons, exclusively located in the VMH, are equipped with receptors that bind various hormonal signals, including leptin [13,14]. Studies have shown that the SF1-specific deletion of various receptors involved in energy homeostasis or their downstream pathways, such as phosphoinositide 3-kinase and AMP-activated protein kinase signaling, predisposes mice to obesity and metabolic syndrome [13–17].

The BBSome is a critical regulator of various cellular and physiological processes, including neuronal function [18]. The BBSome is a large protein complex made up of 8 Bardet–Biedl syndrome (BBS) proteins (BBS1, BBS2, BBS4, BBS5, BBS7, BBS8, BBS9, and BBS18) [19,20].

[1]Department of Neuroscience and Pharmacology, University of Iowa Carver College of Medicine, Iowa City, IA, USA [2]Veterans Affairs Health Care System, Iowa City, IA, USA [3]Department of Internal Medicine, University of Iowa Carver College of Medicine, Iowa City, IA, USA [4]NeurObesity Group, Department of Physiology, CiMUS, University of Santiago de Compostela-Instituto de Investigación Sanitaria, Santiago de Compostela, Spain [5]Obesity Research and Education Initiative, University of Iowa Carver College of Medicine, Iowa City, IA, USA [6]Fraternal Order of Eagles Diabetes Research Center, University of Iowa Carver College of Medicine, Iowa City, IA, USA [7]Iowa Neuroscience Institute, University of Iowa Carver College of Medicine, Iowa City, IA, USA [8]Department of Physiology, Medical College of Wisconsin, Milwaukee, WI, USA

[9] Mohamed Rouabhi and Deng-Fu Guo contributed equally to this work.

*Corresponding author. Department of Neuroscience and Pharmacology, University of Iowa, Roy J. and Lucille A. Carver College of Medicine, 51 Newton Rd., 2-248 BSB, Iowa City, IA, 52242, USA. Fax: +319 353 5350. E-mail: kamal-rahmouni@uiowa.edu (K. Rahmouni).

Received January 22, 2021 • Revision received February 25, 2021 • Accepted March 8, 2021 • Available online 13 March 2021

https://doi.org/10.1016/j.molmet.2021.101211

Abbreviations

AgRP	agouti-related protein
ATGL	adipose triglyceride lipase
BAT	brown adipose tissue
BBS	Bardet-Biedl syndrome
FAS	fatty acid synthase
HR	heart rate
HSL	hormone-sensitive lipase
ICV	intracerebroventricular
LepRb	leptin receptor
MAP	mean arterial pressure
NPY	neuropeptide Y
POMC	proopiomelanocortin
SF1	steroidogenic factor 1
SNA	sympathetic nerve activity
SNS	sympathetic nervous system
STAT3	signal transducer and activator of transcription 3
VMH	hypothalamic ventromedial nucleus
WAT	white adipose tissue

The absence of any BBS protein halts the formation and function of the BBSome. Obesity, including morbid obesity, is highly prevalent in patients carrying mutations in *BBS* genes that disrupt the function of the BBSome [21,22]. Moreover, individuals with BBS tend to have more adiposity, particularly visceral fat, than non-BBS subjects with a comparable body mass index [23]. Similarly, *Bbs* null mice develop obesity and many other cardiometabolic disorders [21,24,25].

In this study, we examined the importance of the SF1 neuron BBSome for the control of energy homeostasis and related physiological processes. We found that selective disruption of the BBSome in SF1 neurons through *Bbs1* gene deletion leads to an increase in body weight and adiposity caused by a decrease in energy expenditure. This was associated with reduction in thermogenic capacity of BAT and increased lipid storage in WAT due to a lower sympathetic tone to both tissues. Notably, disruption of the BBSome in SF1 neurons is associated with normal glucose metabolism, insulin sensitivity, and blood pressure despite obesity and hyperinsulinemia. Our findings highlight the importance of the SF1 neuron BBSome for the control of energy homeostasis and the development of obesity-related comorbidities.

2. MATERIAL AND METHODS

2.1. Animals

To specifically disrupt the BBSome in SF1 neurons, mice bearing the *Bbs1* gene flanked by loxP sites ($Bbs1^{fl/fl}$), on C57BL6 background, were bred with mice expressing Cre recombinase driven by the SF1 promoter ($SF1^{Cre}$, Jackson Laboratory, stock#012462), on a mixed background (129 SvEv, FVB/NJ and C57BL/6 J). To validate the specificity of Cre-dependent activity to the VMH, we used a td-Tomato reporter mouse on a mixed background (129SvEv and C57BL/6 J). This mouse has a stop codon flanked by loxP sites preceding the start position of a td-Tomato locus ($Stop^{fl/fl}$-tdTomato). Cre recombination removes the stop site, leading to td-Tomato fluorescence protein expression that can be visualized under a fluorescence microscope. A male $SF1^{cre}$ mouse was bred with a female $Stop^{fl/fl}$-tdTomato mouse. Genotyping of the mice was determined using standard polymerase chain reaction (PCR). Tail DNA was extracted by using ethanol precipitation, and PCR amplification was performed using primers provided in Table S1. PCR product was assayed in ethidium bromide gel (2% agarose in Tris-acetate-EDTA).

All animal testing was approved by the University of Iowa Animal Care and Use Committee. Mice were maintained on a 12:12-hour light–dark cycle (light off at 6 PM) in temperature (23 °C)-controlled rooms with access to mouse chow (Teklad 7913) and tap water ad libitum.

2.2. Analysis of body weight, adiposity, and food intake

To compile growth curves, we weighed the mice once per week for 25 weeks, from weaning. Magnetic resonance imaging and nuclear magnetic resonance were used to measure body composition (fat and lean mass) in mice. At the end of the experiments, the mice were sacrificed, and their liver; kidneys; BAT; and various fat pads, including perirenal, gonadal, and inguinal WAT, were dissected and weighed. As a marker of body fat mass, we measured circulating leptin. To achieve this objective, we obtained plasma by using 0.5 M EDTA (25 μl) and centrifugation from blood acquired during the sacrifice of the mice. Leptin concentration was measured by using a mouse leptin ELISA kit (RayBiotech). To measure food intake, we housed the mice in individual cages. After 3 days of acclimation to individual housing, daily and cumulative food intake were measured over a 4-day period.

2.3. Comprehensive phenotyping system

The PromethION system (Sable Systems International) was used to simultaneously measure energy expenditure, respiratory exchange ratio, food intake, and ambulatory activity. This system comprises 16 metabolic cages similar to home cages with bedding. Mice (aged 7–9 weeks) were acclimated to the new environment for 2 days before the 24-hour measurements were performed during 2 consecutive days. Heat production was estimated from the respiratory gas exchange by using the modified Weir equation [27,28]. The respiratory exchange ratio was calculated as the ratio of CO_2 produced (VCO_2) versus O_2 consumed (VO_2).

2.4. Bomb calorimetry

Feces were collected from mice housed in individual metabolic cages designed to study metabolic and fluid balance (model 3600M021, Techniplast USA). Mice (aged 7–9 weeks) were acclimated to the cages for 2 days before the 24-hour collection of feces along, and food intake measurements were performed. Caloric densities of food and fecal samples were determined by using a semimicro bomb calorimeter (Parr Instrument Company). Caloric absorption was calculated by subtracting the calories lost to feces from the calories consumed. Digestive efficiency represents the percentage of calories absorbed relative to the calories consumed.

2.5. Glucose and insulin tolerance tests

A glucose tolerance test was performed in overnight fasted obese $SF1^{Cre}/Bbs1^{fl/fl}$ mice and littermate controls (aged 24–26 weeks). Blood samples were taken from the tail to measure blood glucose at baseline, and then mice were injected intraperitoneally (i.p.) with glucose (Sigma–Aldrich, 2 mg/kg body weight). To test for the glucose-reducing effect of insulin, we fasted the mice for 5 hours. Next, baseline glucose levels were measured, and the mice were injected i.p. with insulin (Novo Nordisk, 0.5 unit/kg body weight). Blood glucose was measured 15, 30, 60, and 120 minutes after injection of glucose or insulin. Blood glucose levels were determined by a glucometer (One Touch Ultra 1, LifeScan Inc.). Plasma obtained by centrifuging blood collected in 25 μl of 0.5 M EDTA was used to measure insulin with an ELISA kit (RayBiotech).

2.6. Intracerebroventricular (ICV) cannulation

Mice were anesthetized with isoflurane (5% for induction; 1%—2% to sustain). Once anesthetized, each mouse was placed in a stereotaxic device and implanted with a stainless-steel cannula (25G, 9 mm length) into the lateral brain ventricle (0.3 mm posterior and 1.0 mm lateral to bregma and 3.0 mm below the surface of the skull). Mice were allowed to recover for 7—10 days.

2.7. Sympathetic nerve recording

Regional sympathetic nerve activity (SNA) was measured using direct multifiber recording in anesthetized mice, as described [33]. Mice were anesthetized with i.p. injection of ketamine (91 mg/kg) and xylazine (9.1 mg/kg). Each mouse was intubated (PE-50) to allow for spontaneous respiration of oxygen-enriched room air. Body temperature, measured with a rectal probe, was kept constant at 37.5 °C by using a surgical heat lamp and a metal heat platform. The left jugular vein was cannulated with a micro-renathane tubing (MRE-40) to sustain the level of anesthesia throughout the 4-hour protocol with α-chloralose (initial dose: 12 mg/kg; sustaining dose of 6 mg/kg/h) and for drug treatments. Finally, the left carotid artery was cannulated with a tapered micro-renathane tubing (MRE-40) for continuous measurement of arterial pressure and heart rate.

A dissecting microscope was employed: the nerve subserving BAT, inguinal WAT, hindlimb (lumbar SNA), visceral organs (splanchnic SNA), or left kidney (renal SNA) was identified, carefully dissected free, and placed on a bipolar 36-gauge platinum-iridium electrode (A-M Systems). When the optimum recording of SNA was obtained from each nerve, the electrode was covered with silicone gel (Kwik-Sil; World Precision Instruments Inc). The electrode was attached to a high-impedance probe (HIP-511, Grass Instruments), and the nerve signal was amplified 10^5 times with a Grass P5 AC pre-amplifier. The amplified nerve signal was filtered at a 100-Hz and 1000-Hz cutoff with a nerve traffic analysis system (model 706C, University of Iowa Bioengineering). The amplified and filtered nerve signal was routed to a speaker system and to an oscilloscope (model 54501 A, Hewlett—Packard) to monitor the audio and visual quality of the sympathetic and parasympathetic nerve recordings and for quantification purposes. The amplified, filtered nerve signal was also directed to a MacLab analogue-digital converter (Model 8 S, AD Instruments Castle Hill) containing software (MacLab Chart Pro; Version 7.0) that uses a cursor to analyze the number of spikes/second that exceeds the background noise threshold.

Baseline BAT, WAT, and SNA were recorded at a young age (aged 5—7 weeks); lumbar, splanchnic, and renal SNA were measured in older (aged 25—26 weeks) mice. All baseline SNA recordings were performed during a 30-minute period at a stable core body temperature of 37.5 °C. The effect of cooling on BAT SNA was tested after baseline BAT SNA was obtained, and the core body temperature of each mouse was gradually lowered over a 40-minute period (to achieve a temperature drop of approximately 0.25 °C/min). Cooling of the mouse was performed by first extinguishing all the heat sources (surgical heat lamp and metal heat platform) and then placing chemical ice packs (pre-cooled at −80 °C) on the metal platform to indirectly cool the mouse. SNA was recorded continuously during the decrease in body temperature. To examine the effect of leptin, we recorded BAT SNA during the 10—15-minute baseline before the ICV injection of leptin (2 μg). BAT SNA was followed for the next 4 hours.

Arterial baroreflex control of renal SNA was tested by intravenous infusion of sodium nitroprusside (at doses of 0.05, 0.1, 0.5, and 1 μg) followed by phenylephrine (at doses of 0.05, 0.1, 0.5, and 1 μg), which decreases and increases arterial pressure, respectively. To ensure that background electrical noise was excluded from sympathetic measurements, post-mortem background activity was subtracted from all SNA.

2.8. Radiotelemetry measurements

Arterial pressure and heart rate were recorded in obese $SF1^{Cre}/Bbs1^{fl/fl}$ mice and littermate controls (aged 24—26 weeks) by using a continuous radiotelemetric measurement (Data Science Instruments). Animals were anesthetized with isoflurane (up to 5% for induction, 1.5%—2% for maintenance). Under aseptic surgical conditions, the catheter of the telemeter was inserted into the left carotid artery and tied securely using a silk suture. The transmitter was placed into a subcutaneous pocket in the mid-abdominal region. Mice were allowed to recover for 7—10 days before arterial pressure and heart rate were recorded continuously in the conscious, unrestrained state for 5—7 days. Hemodynamic parameters were recorded for 10 seconds every 5 minutes and stored on a personal computer using Data Science Dataquest software.

2.9. Power spectral analysis of blood pressure and heart rate

At the end of the basal telemetry recording, spectral analysis for blood pressure and heart rate variability was performed. The configuration for sequential telemetry data acquisition was changed to a single, continuous recording at a rate of 2000 Hz for 60 min for each mouse during the daytime hours (9 AM—3 PM). This increase in sampling frequency allowed a beat-by-beat heart rate time series to be derived from the blood pressure waveforms and converted to an equidistant sampling rate using cubic spline interpolation. Those equidistant heart rate time series were subjected to a fast Fourier transform to calculate spectral power in the very low frequency (VLF, 0.02—0.20 Hz), low frequency (LF, 0.2—1.0 Hz, reflecting mainly sympathetic cardiac modulation), and high frequency (HF, 1.0 ± 0.5 Hz, reflecting parasympathetic cardiac modulation) bands. Relative LF and HF were calculated as the relative value of each power component in proportion to the total power minus the VLF component. The LF/HR ratio of heart rate variability was used as an indication of SNA to the heart; the LF component of the arterial pressure was used as an indication of SNA in vascular tone regulation. Baroreceptor reflex sensitivity was determined from the blood pressure recording using the sequence technique. Spectral analysis and baroreflex testing were performed with HemoLab software, freely available at http://www.haraldstauss.com/HaraldStaussScientific/products/default.html.

2.10. Surface body temperature measurement

The surface body temperature of mice aged 7—9 weeks was recorded by using a high-resolution infrared camera (A655sc Thermal Imager; FLIR Systems). Quantitative analysis of infrared images was performed with FLIR ResearchIR software version 3.4.13039.1003. Mice were imaged side by side to allow simultaneous assessment and direct comparison of the body surface temperature between the $SF1^{Cre}/Bbs1^{fl/fl}$ mice and control mice.

2.11. Immunofluorescence

Mice (aged 7—9 weeks) were fasted overnight and treated with leptin (2 mg/kg, i.p.) 2 hours before they were anesthetized with ketamine (91 mg/kg) and xylazine (9.1 mg/kg) and then perfused with phosphate-buffered saline (PBS, 5 mL/min; 20 mL) followed by 4% paraformaldehyde/HistoChoice Tissue Fixative (Amresco) in PBS (3 mL/min; 45 mL). The excised brain was incubated in the same fixative overnight at 4 °C and then washed 3 times with PBS and incubated in 30% sucrose/PBS. Brains were vibratome-sectioned with 30 μm thickness. Immunochemistry was performed on brain sections

by using antibodies against phosphorylated Stat3 (p-Stat3, 1:250, #9131 S, Cell Signaling), as described [26]. Processed brain sections were mounted by using VectaShield® mounting medium with 4', 6-diamidino-2-phenylindole (DAPI). Images were visualized by using confocal microscopy (Zeiss LSM710). The intensity of p-Stat3 staining in defined nuclei was quantified by using Image J software.

2.12. Western blotting

Samples of protein extracts were combined with an equal volume of sodium dodecyl sulfate sample buffer. Samples were resolved on 9% polyacrylamide gels, and the separated proteins transferred to polyvinylidene difluoride membranes. Membranes were probed with antibodies against uncoupling protein 1 (UCP1, 1:1,000, #sc-6528, Santa Cruz Biotechnology), hormone-sensitive lipase (HSL, 1,000, #4107, Cell Signaling), phospho-HSL (1:1,000, #4139, Cell Signaling), adipose triglyceride lipase (ATGL, 1:1,000, #2439, Cell Signaling), fatty acid synthase (FAS, 1:2,500, #610962, BD Transduction Laboratories), or β-actin (60008-I-Ig, 1:50,000, Proteintech) followed by a secondary anti-rabbit antibody (1:10,000, #7074, Cell Signaling), anti-mouse antibody (1:10,000, #7076, Cell Signaling), or anti-goat antibody (1:1,000, #sc-2354, Santa Cruz Biotechnology). The protein level was visualized with an enhanced chemiluminescent detection kit (GE healthcare) and quantified by using ImageJ software.

2.13. Gene expression

Mice were sacrificed by CO_2 asphyxiation, and each brain was quickly isolated and placed on ice. Hypothalamic nuclei and tissue of interest were carefully dissected, and RNA was isolated by using the RNeasy Plus Mini Kit from Qiagen. Total RNA (2 μg in a final volume of 40 μL) was used to synthesize first-strand cDNAs with the Super-Script preamplification system. Next, 10 μL of cDNA and 0.4 mmol/L of primers were added in a final volume of 25 μL PCR mixture (iQ SYBR Green supermix, Bio-Rad) and amplified in an iQ5 Multicolor Real Time PCR Detection System (Bio-Rad). The PCR conditions for all genes were as follows: denaturation for 5 minutes at 95 °C and then 40 cycles for 30 s at 95 °C and 30 s at 60 °C. Notably, 18 S ribosomal RNA expression was used as an internal control to normalize mRNA expression of these genes. The $2^{-\Delta\Delta CT}$ method was used to calculate the relative fold gene expression. Primer sequences are provided in Table S1.

2.14. Statistical analysis

Data are expressed as means ± standard error of the mean. Student's t test or analysis of variance (ANOVA) was used to test for differences. A one-way ANOVA was used in cases where 3 groups were analyzed. A two-way ANOVA with or without repeated measures was used if multiple groups and multiple variables were present. Univariate regression modeling with body weight considered as a covariate was used to assess energy expenditure data by using SPSS. $p < 0.05$ was considered significant.

3. RESULTS

3.1. *Bbs1* gene deletion in the SF1 neurons alter leptin sensitivity

To examine the importance of the BBSome in the VMH, we assessed the effects of *Bbs1* gene deletion from SF1 neurons. To achieve this objective, we crossed the $SF1^{Cre}$ mice that provide the specificity of Cre expression to the VMH with $Bbs1^{fl/fl}$ mice. The use of a reporter mouse model expressing fluorescent td-Tomato to visualize Cre activity confirmed its restriction to the VMH (Figure 1A). Moreover, *Bbs1* gene expression was substantially reduced in the VMH of $SF1^{Cre}$/$Bbs1^{fl/fl}$ mice relative to littermate controls (Figure 1B). However, *Bbs1* gene expression was not altered in other brain regions such as the hippocampus or cortex of $SF1^{Cre}$/$Bbs1^{fl/fl}$ mice. Moreover, leptin-induced activation of Stat3 was blunted in the VMH of the $SF1^{Cre}$/$Bbs1^{fl/fl}$ mice (Figure 1C,D), which is consistent with our findings implicating the BBSome in leptin sensitivity by mediating the trafficking of the leptin receptor (LepRb) [18,26,27]. By contrast, the leptin-evoked increase in phospho-Stat3 in the arcuate nucleus of the hypothalamus was not altered in $SF1^{Cre}$/$Bbs1^{fl/fl}$ mice relative to controls (Figure 1C,E), demonstrating the functional specificity of the deletion to the VMH.

We have demonstrated that global null BBS mice and mice carrying *Bbs1* gene deletion in LepRb-expressing neurons or proopiomelanocortin (POMC) neurons have lower POMC expression in the arcuate nucleus [18,24,26,27]. However, $SF1^{Cre}$/$Bbs1^{fl/fl}$ mice displayed no change in arcuate nucleus POMC mRNA levels (Fig. S1). Expression levels of neuropeptide Y (NPY) and agouti-related protein (AgRP) were also comparable between $SF1^{Cre}$/$Bbs1^{fl/fl}$ and control mice. Collectively, these findings confirm the specificity of *Bbs1* gene deletion to the VMH of $SF1^{Cre}$/$Bbs1^{fl/fl}$ mice.

3.2. Disruption of SF1 neuron *Bbs1* gene cause obesity

Analysis of growth curves showed that until 7 weeks of age, male and female $SF1^{Cre}$/$Bbs1^{fl/fl}$ mice have comparable body weight with littermate controls (Figure 2A,B). However, after 7 weeks of age, $SF1^{Cre}$/$Bbs1^{fl/fl}$ mice begin gaining more weight than their littermate controls do. Notably, heterozygous ($SF1^{Cre}$/$Bbs1^{wt/fl}$) mice without 1 copy of the *Bbs1* gene in SF1 neurons had intermediate body weight: at the end of study (aged 25 weeks), the body weight of heterozygous mice (males: 41.1 ± 2.2 g and females: 29.4 ± 1.0 g) was in between that of control animals (males: 36.7 ± 1.7 g and females: 25.7 ± 2.2 g) and homozygous mice (males: 43.2 ± 2.8 g and females: 31.3 ± 2.9 g).

The increased body weight of $SF1^{Cre}$/$Bbs1^{fl/fl}$ mice was due to an increase in fat mass. Notably, fat mass was significantly elevated in $SF1^{Cre}$/$Bbs1^{fl/fl}$ relative to control littermates (Figure 2C,D). In line with this finding, $SF1^{Cre}$/$Bbs1^{fl/fl}$ mice displayed elevated plasma leptin (Figs. S2A and C) and elevated weight of inguinal, gonadal, and renal fat depots (Figs. S2B and D). Consistent with body weight data, the fat mass of heterozygous $SF1^{Cre}$/$Bbs1^{wt/fl}$ mice was intermediate between homozygous and control mice. A significant increase in liver mass was observed in $SF1^{Cre}$/$Bbs1^{fl/fl}$ mice, and a trend was observed in heterozygous $SF1^{Cre}$/$Bbs1^{wt/fl}$ mice (Figs. S2B and D). However, there was no difference in lean mass between the homozygous, heterozygous, and control mice (Figure 2E). This finding was further supported because no difference was observed in the weight of the kidneys (Figs. S2B and D). These findings indicate that disruption of the BBSome in SF1 neurons is sufficient to cause obesity.

3.3. SF1 neuron *Bbs1* gene deletion does not alter glucose homeostasis and insulin sensitivity

Circulating insulin was significantly elevated in $SF1^{Cre}$/$Bbs1^{fl/fl}$ mice (Fig. S3A). However, fasting blood glucose levels were not different in $SF1^{Cre}$/$Bbs1^{fl/fl}$ mice (males: 77.8 ± 3.7 mg/dL and females: 67.5 ± 3.8 mg/dL) and littermate controls (males: 81.2 ± 5.3 mg/dL and females: 63.9 ± 3.6 mg/dL; Figs. S3B and D). The glucose tolerance test showed that $SF1^{Cre}$/$Bbs1^{fl/fl}$ mice tend to be glucose-intolerant; however, this was not statistically significant (Figs. S3B and D). This finding was further confirmed by the calculation of the area under the curve (Figs. S3C and E). We also performed an insulin tolerance test, which revealed no significant difference in insulin sensitivity between $SF1^{Cre}$/$Bbs1^{fl/fl}$ mice and controls (Figs. S3F–I).

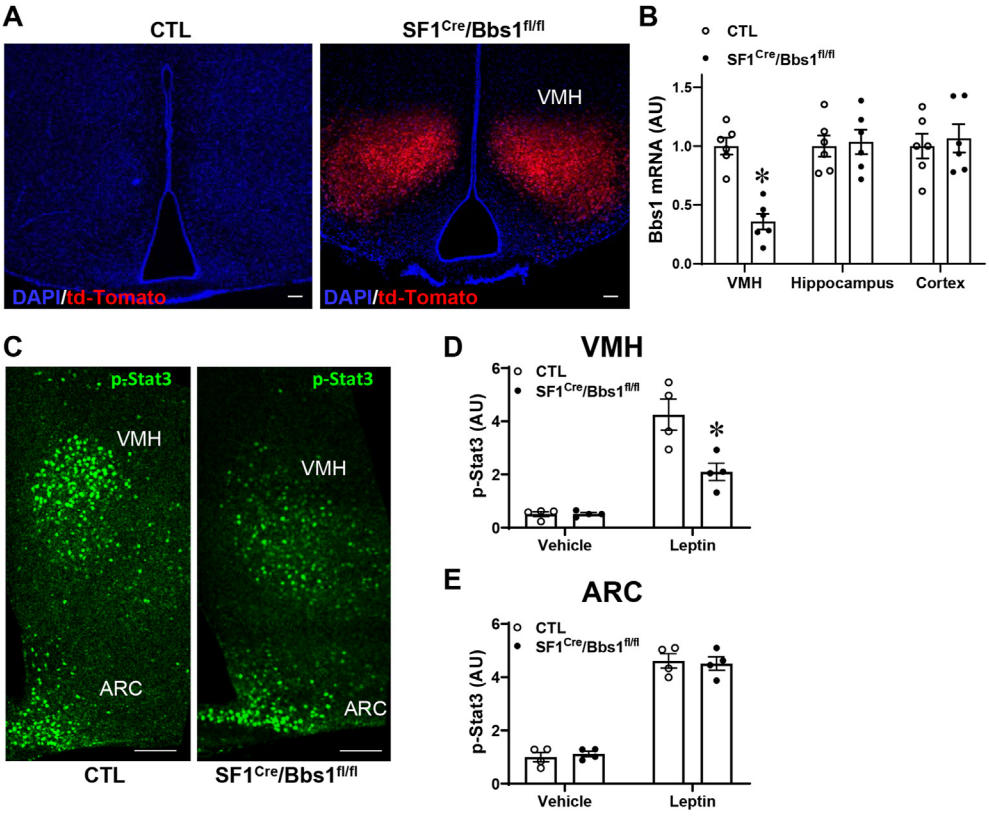

Figure 1: Validation and specificity of *Bbs1* gene deletion in VMH SF1 neurons in SF1^{Cre}/Bbs1$^{fl/fl}$ mice. (A) Evidence of Cre recombinase (presence of red fluorescent td-Tomato) in the VMH of SF1^{Cre}/Stop$^{fl/fl}$-tdTomato reporter, but not control, mice. (B) Reduction in *Bbs1* gene expression in the VMH, but not in the hippocampus or cortex, of SF1^{Cre}/Bbs1$^{fl/fl}$ mice. (C–E) Blunted leptin-induced increase in phospho-Stat3 in the VMH, but not arcuate nucleus (ARC), of SF1^{Cre}/Bbs1$^{fl/fl}$ mice. *P $<$ 0.05 vs. control (CTL, B) or CTL + leptin (D).

Thus, despite causing obesity and hyperinsulinemia, SF1 neuron-specific disruption of the BBSome does not alter glucose metabolism and insulin sensitivity.

3.4. SF1 neuron BBSome is required for the control of energy expenditure

To understand the processes underlying the obesity phenotype caused by SF1 neuron *Bbs1* gene ablation, we evaluated energy intake and expenditure during the developmental phase of obesity (aged 7–9 weeks). The amount of chow consumed by male and female SF1^{Cre}/Bbs1$^{fl/fl}$ mice housed in their home cage was comparable to that eaten by littermate controls (Figure 3A,B). Similarly, food intake measured in metabolic cages was the same in SF1^{Cre}/Bbs1$^{fl/fl}$ mice and the controls (Figs. S4A and B). We also compared food intake between older (aged 24–26 weeks) obese SF1^{Cre}/Bbs1$^{fl/fl}$ mice and controls but found no difference (Figs. S5A–B). Measurement of energy absorption and digestive efficiency revealed no differences between SF1^{Cre}/Bbs1$^{fl/fl}$ mice and controls (Figure 3C,D).

Next, we assessed energy expenditure by respirometry. Regression analysis revealed a significant effect of genotype upon energy expenditure during the dark phase (Figure 4A–B). The reduced energy expenditure in SF1^{Cre}/Bbs1$^{fl/fl}$ mice was confirmed when analysis of covariance (ANCOVA) was applied (Figure 4C), but that this is not due to changes in substrate utilization as demonstrated by similar respiratory exchange ratio (Figs. S6A and C) nor changes in ambulatory activity (Figs. S4C and D and Figs. S6B and D). Collectively, these results point to a decrease in energy expenditure as the main cause of obesity in mice with the *Bbs1* gene in SF1 neurons.

3.5. SNS-mediated control of BAT and WAT by SF1 neuron involves the BBSome

The importance of BAT in mediating the control of energy expenditure by SF1 neurons [17,28] led us to measure markers of thermogenesis in this tissue during the developmental phase of obesity (aged 7–9 weeks). Using thermographic imaging analysis, we found that SF1^{Cre}/Bbs1$^{fl/fl}$ mice have lower skin temperature in the BAT area (Figure 4D–E), which is consistent with the decreased energy expenditure. This finding is further supported by the reduced UCP1 protein expression levels in BAT of SF1^{Cre}/Bbs1$^{fl/fl}$ mice (Figure 5A). The SNS is a critical component in linking SF1 neurons to BAT, and direct sympathetic nerve recording revealed a significantly lower BAT sympathetic nerve traffic in SF1^{Cre}/Bbs1$^{fl/fl}$ mice (Figure 5B). Moreover, the increase in BAT SNA evoked by cooling was substantially blunted in SF1^{Cre}/Bbs1$^{fl/fl}$ mice (Figure 5C). Leptin-induced BAT sympathetic nerve activation was also reduced in the SF1^{Cre}/Bbs1$^{fl/fl}$ mice (Figure 5D). These findings indicate that disruption of the BBSome in SF1 neurons decreases the thermogenic activity of BAT through sympathetic inhibition. Similar to BAT SNA, inguinal WAT SNA was significantly lower in SF1^{Cre}/Bbs1$^{fl/fl}$ mice than in the controls (Figure 5E). To determine the relevance of this finding, we measured the expression levels of proteins involved in lipid storage and metabolism. We focused on the

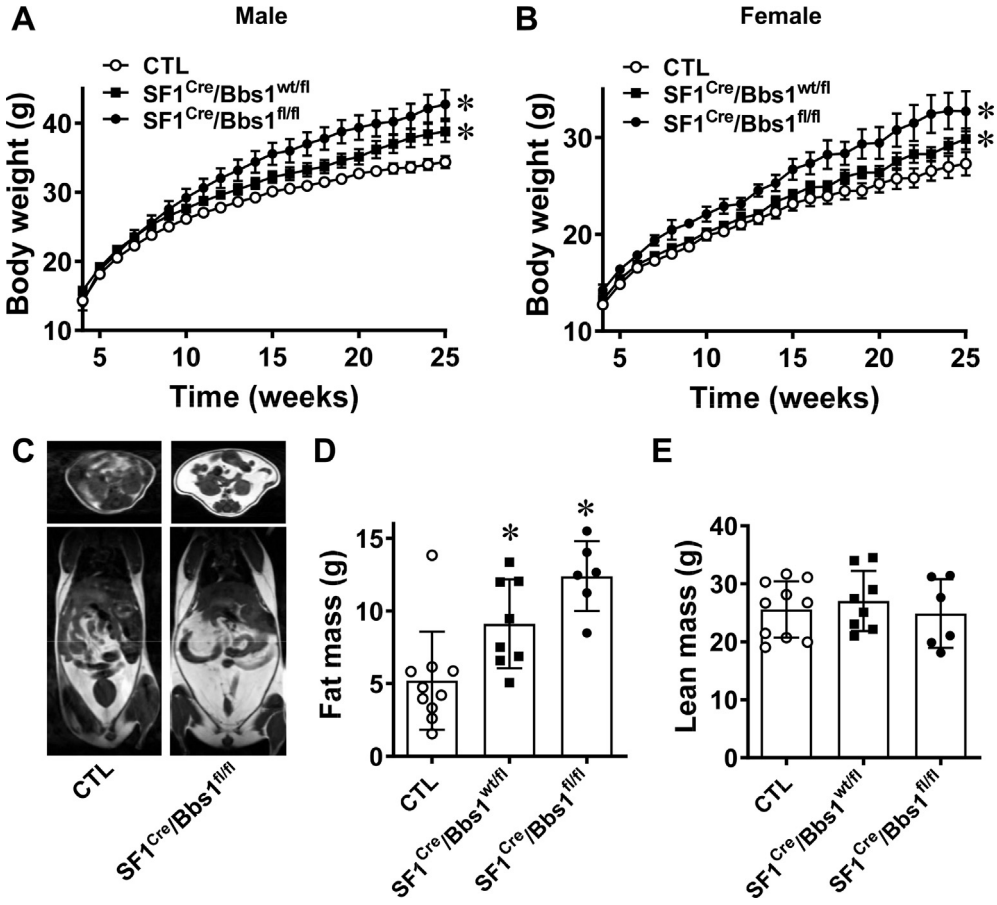

Figure 2: Effects of SF1 neuron *Bbs1* gene deletion on body weight and adiposity. (A, B) Weekly body weights of male (A) and female (B) mice (n = 38 males and 26 females for control (CTL) mice, 19 males and 14 females for $SF1^{cre}/Bbs1^{fl/fl}$ mice, and 13 males and 9 females for $SF1^{cre}/Bbs1^{wt/fl}$ mice). (C) Representative images of vertical and horizontal cross-sections of mice showing visible differences in adiposity. (D, E) NMR-quantified fat mass and lean mass. *P < 0.05 vs. control group.

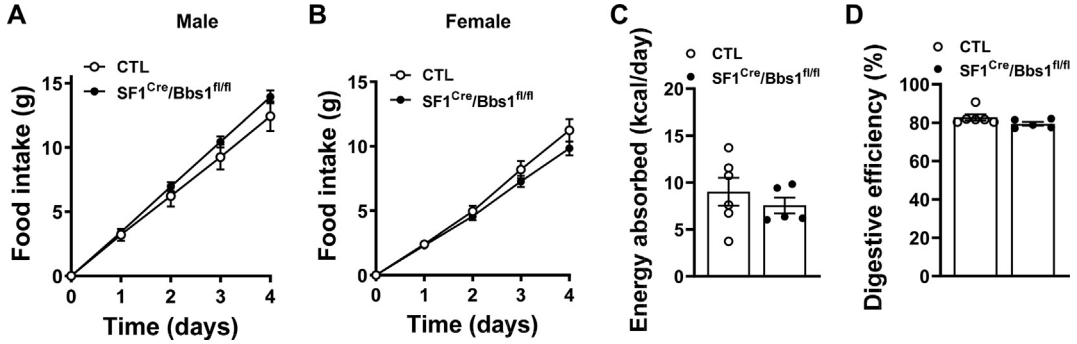

Figure 3: Effect of SF1 neuron *Bbs1* gene deletion on energy intake in young mice. (A, B) Cumulative daily food intake (n = 12 males and 10 females for control [CTL] and 19 males and 18 females for $SF1^{cre}/Bbs1^{fl/fl}$ mice). (C, D) Energy absorption and digestive efficiency. n = 5–6.

expression of FAS that mediates de novo lipogenesis and ATGL and the phosphorylated level of HSL, 2 major rate-determining enzymes in adipocyte lipolysis. Notably, the levels of FAS were elevated, and the levels of ATGL and phospho-HSL were significantly lower in the WAT of $SF1^{Cre}/Bbs1^{fl/fl}$ mice than in the controls (Figure 5F). Overall, these data are consistent with the critical role of the SNS in adipose tissue physiology. The changes in WAT observed in $SF1^{Cre}/Bbs1^{fl/fl}$ mice promote lipid storage, which is consistent with the increased adiposity in these animals.

3.6. Differential effect of SF1 neuron BBSome disruption on regional SNS activity

Next, we investigated whether the obesity evoked by SF1 neuron *Bbs1* gene deletion affects the cardiovascular sympathetic traffic. Notably, splanchnic SNA was significantly elevated in obese $SF1^{Cre}/Bbs1^{fl/fl}$ mice relative to the controls (Figure 6A). This increase in baseline splanchnic SNA in $SF1^{Cre}/Bbs1^{fl/fl}$ mice was present in both males (38 ± 6 vs. 27 ± 3 spikes/s, $p < 0.05$) and females (53 ± 6 vs. 24 ± 1 spikes/s, $p < 0.05$). Moreover, $SF1^{Cre}/Bbs1^{fl/fl}$ mice displayed

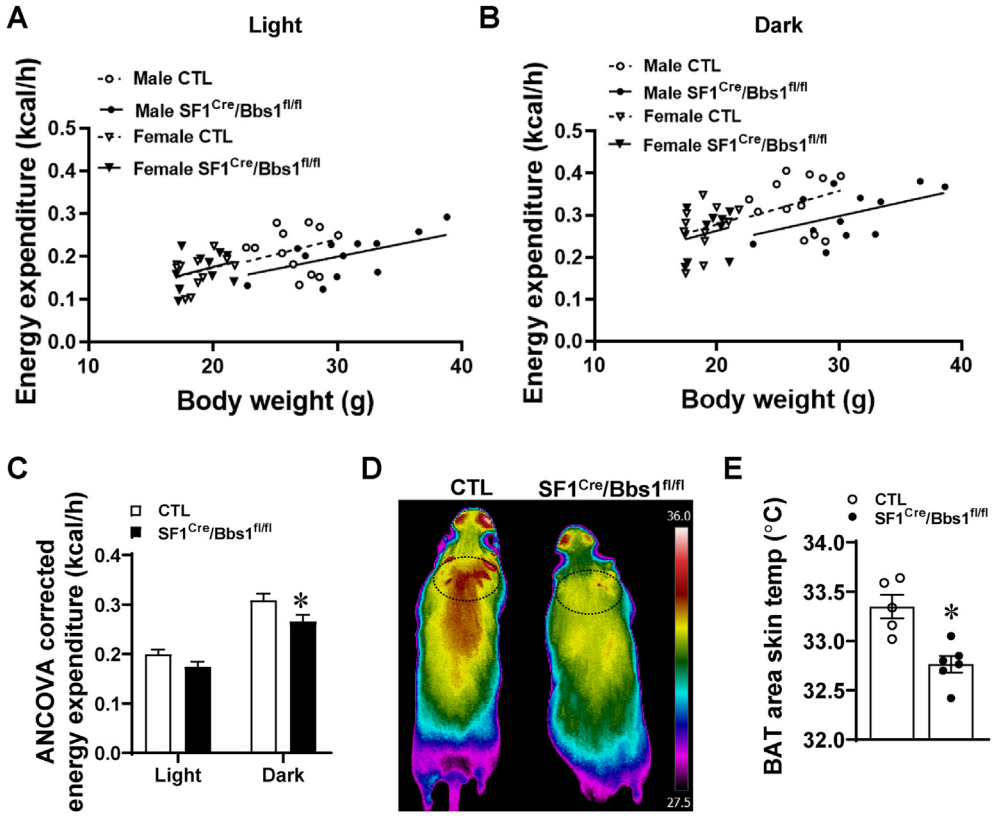

Figure 4: Effect of SF1 neuron *Bbs1* gene deletion on energy expenditure. (A) Aerobic energy expenditure during the light phase. Generalized linear modeling: $P_{Model} = 0.002$, $P_{Intercept} = 0.687$, $P_{Body\ Mass} = 0.011$, $P_{Genotype} = 0.093$, $P_{Sex} = 0.516$, $P_{Genotype\ x\ Sex} = 0.201$. (B) Aerobic energy expenditure during the dark phase. Generalized linear modeling: $P_{Model} = 0.003$, $P_{Intercept} = 0.197$, $P_{Body\ Mass} = 0.034$, $P_{Genotype} = 0.028$, $P_{Sex} = 0.757$, $P_{Genotype\ x\ Sex} = 0.367$. (C) Estimated marginal means from generalized linear models in (A) and (B), calculated at global mean body masses of 24 g. (D–E) Representative images of skin temperature in the BAT area (D) and quantification data (E). *$P < 0.05$ vs control (CTL) group.

elevated efferent nerve activity, measured distal to the recording site after transection of the nerve (41 ± 7 vs. 22 ± 3 spikes/s, $p < 0.05$). Lumbar SNA and renal SNA were not different in obese SF1^{Cre}/Bbs1$^{fl/fl}$ mice relative to the controls (Figure 6B,C). These findings demonstrate that regional SNA is differentially affected by SF1 neuron *Bbs1* gene deletion.

3.7. Cardiovascular autonomic effects of SF1 neuron BBSome disruption

Finally, we tested whether obese SF1^{Cre}/Bbs1$^{fl/fl}$ mice display changes in arterial pressure and autonomic function. Notably, obese SF1^{Cre}/Bbs1$^{fl/fl}$ mice (body weight: 38.63 ± 1.81 g vs. 27.82 ± 1.15 g in the control group) displayed no significant changes in mean (MAP), systolic, or diastolic arterial pressure relative to control mice (Figure 6D and Figs. S7A–C). This absence of change in blood pressure was observed in males (MAP: 98 ± 4 mmHg in SF1^{Cre}/Bbs1$^{fl/fl}$ mice (n = 4) vs. 95 ± 1 mmHg in controls (n = 3)) and females (MAP: 97 ± 2 mmHg in SF1^{Cre}/Bbs1$^{fl/fl}$ mice (n = 5) vs. 94 ± 3 mmHg in controls (n = 4)). Heart rate was also comparable between obese SF1^{Cre}/Bbs1$^{fl/fl}$ and control mice (Figure 6E and Fig. S7D). Moreover, analysis of variability of blood pressure and heart rate, widely used as indices of cardiac sympatho-vagal balance and cardiac parasympathetic reflex control, showed no difference between SF1^{Cre}/Bbs1$^{fl/fl}$ and control mice (Figs. S8A–B). Similarly, the power spectral analysis of baroreflex sensitivity that uses the normal, physiological fluctuations of blood pressure and cardiac intervals that occur over time revealed no change in SF1^{Cre}/Bbs1$^{fl/fl}$ mice relative to controls (Fig. S8C). Measurement of the response of renal SNA to changes in arterial pressure evoked by infusion of sodium nitroprusside and phenylephrine confirmed the absence of alteration in baroreflex sensitivity in obese SF1^{Cre}/Bbs1$^{fl/fl}$ mice (Figure 6F). Collectively, these data indicate that loss of the BBSome in SF1 neurons does not alter blood pressure despite increasing fat mass.

4. DISCUSSION

Our study demonstrates that the BBSome in SF1 neurons is an important component in the control of energy homeostasis and obesity-associated impairment in glucose metabolism, baroreflex sensitivity and hypertension. Notably, mice carrying SF1 neuron BBSome disruption through *Bbs1* gene deletion have increased body weight and fat mass under normal chow conditions. In addition, our data show that mice without 1 copy of the *Bbs1* gene in the SF1 neurons develop an intermediate body weight phenotype relative to control and homozygous animals. We also demonstrated that the increase in adiposity in SF1^{Cre}/Bbs1$^{fl/fl}$ mice is mainly driven by a decrease in energy expenditure, because food intake, energy absorption, and digestive efficiency were not altered. This finding is further supported by the reduced markers of thermogenesis and sympathetic traffic in the BAT of SF1^{Cre}/Bbs1$^{fl/fl}$ mice. In addition, SF1^{Cre}/Bbs1$^{fl/fl}$ mice have reduced sympathetic traffic to WAT coupled with a protein expression profile that promotes lipid storage. Notably,

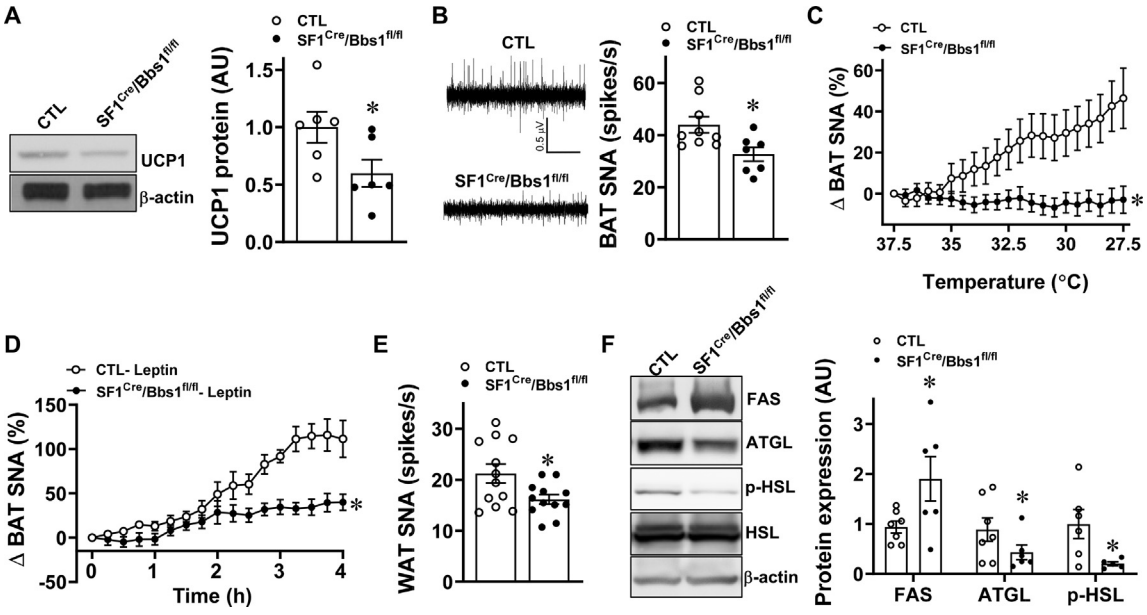

Figure 5: Effect of SF1 neuron *Bbs1* gene deletion on markers of thermogenesis and fat metabolism. (A) Expression level of BAT UCP1 protein (representative Western blots and quantification data are shown). (B) Baseline brown adipose tissue (BAT) sympathetic nerve activity (SNA; representative neurograms and quantification data are shown). (C–D) BAT SNA response to cooling (C, n = 15 for SF1^{cre}/Bbs1$^{fl/fl}$ mice and 16 for controls [CTL]) and 2 μg leptin ICV (D, n = 6 each). (E) Baseline WAT SNA. (F) Expression levels of FAS, ATGL, HSL, and phospho-HSL in WAT (representative Western blots and quantification data are shown, n = 5–6 SF1^{cre}/Bbs1$^{fl/fl}$ mice and 5–6 for CTL). *P < 0.05 vs. CTL group.

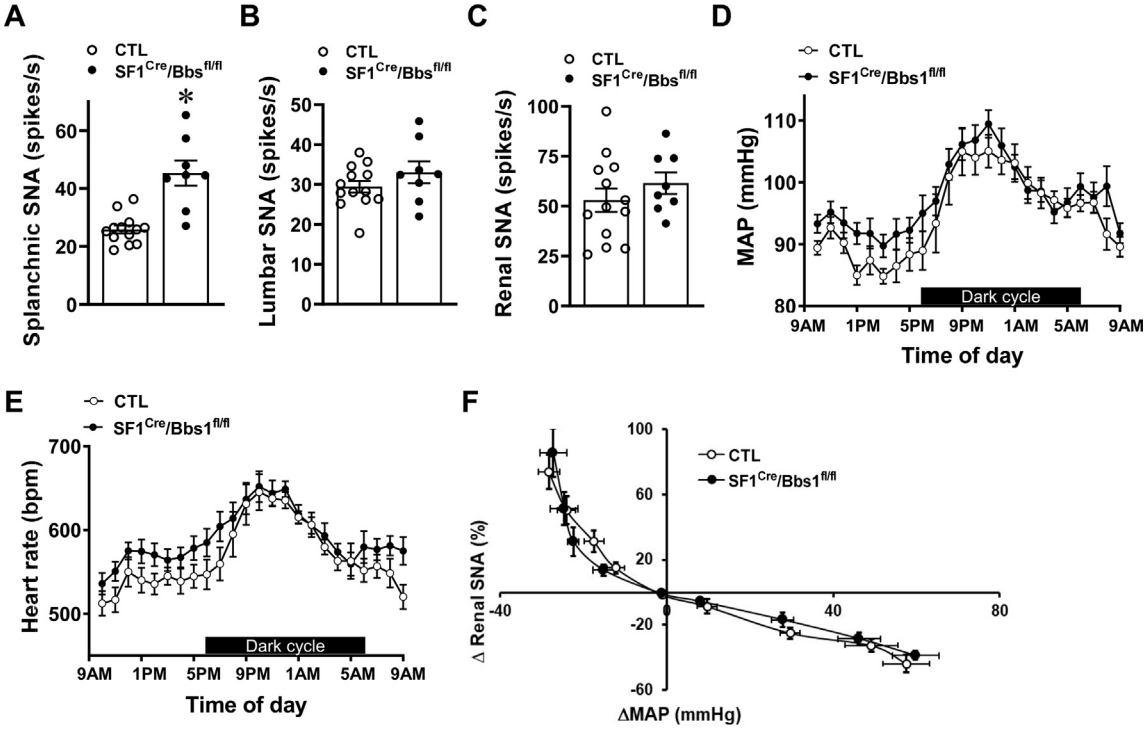

Figure 6: Effect of SF1 neuron *Bbs1* gene deletion on autonomic and cardiovascular functions. (A–C) Baseline splanchnic (A), lumbar (B), and renal (C) sympathetic nerve activity (SNA). (D–G) Hourly mean arterial pressure (MAP, D) and heart rate (HR, E). (n = 7 controls [CTL, 3 males and 4 females] and 9 SF1^{Cre}/Bbs1$^{fl/fl}$ mice [4 males and 5 females]; data analyzed with 2-way ANOVA with repeated measure) (F) Baroreflex sensitivity determined by the response of renal SNA to changes in arterial pressure evoked by sodium nitroprusside and phenylephrine. (n = 6 CTL [3 males and 3 females] and 5 SF1^{Cre}/Bbs1$^{fl/fl}$ mice [4 males and 1 female]; data analyzed with 2-way ANOVA with repeated measure). *P < 0.05 vs. CTL group.

despite the increased body weight, adiposity and hyperinsulinemia SF1^{Cre}/Bbs1$^{fl/fl}$ mice displayed no significant changes in glucose metabolism, insulin sensitivity, baroreflex sensitivity, and blood pressure. This finding shows the requirement of the SF1 neuron BBSome for the development of comorbidities associated with obesity.

Our findings support the notion that the neuronal BBSome plays a critical role in the control of body weight and adiposity in a manner independent of energy intake. This finding contrasts with our prior observations in global *Bbs* null mice and mice without the *Bbs1* gene in the nervous system or LepRb-containing neurons, which display an obese phenotype driven by both an increase in food intake and a decrease in energy expenditure [18,25–27]. The SF1 neuron BBSome appears to influence energy expenditure and lipid accumulation through modulation of the activity of the SNS. Our data show that loss of the BBSome in SF1 neurons leads to reduced sympathetic nerve traffic to BAT and WAT. Notably, the absence of BAT sympathetic activation in response to cooling could explain the lower baseline BAT SNA in SF1^{Cre}/Bbs1$^{fl/fl}$ mice. This is because the housing temperature (23 °C) is cold for mice [29]. Thus, a possibility is that the lower baseline BAT SNA in SF1^{Cre}/Bbs1$^{fl/fl}$ mice results from the inability of these animals to respond to continuous exposure to low temperature. Additional studies using thermoneutral conditions are necessary to assess such possibility.

Importantly, we show that the lower BAT and WAT SNA in SF1^{Cre}/Bbs1$^{fl/fl}$ mice were associated with molecular changes that promote reduced thermogenesis and fat accumulation. These findings point to the BBSome as a novel mechanism by which SF1 neurons control the SNA that regulates peripheral metabolic processes. Further analysis is necessary to define the connection between the BBSome and other cellular mechanisms implicated in the sympathetic control of BAT and WAT activity by SF1 neurons such as AMPK [14,17] or SF1 [12].

Compelling evidence indicates that the BBSome mediates the control of energy balance through its involvement in the trafficking of various receptors to cilia and the plasma membrane. The requirement of the BBSome for the trafficking of the LepRb has particularly emerged as a novel mechanism of leptin resistance and a major cause of obesity in BBS [18,25,26]. Consistent with this concept, we show that loss of the *Bbs1* gene in SF1 neurons leads to a significant reduction in leptin's ability to activate Stat3. This finding is also supported by the studies showing that LepR deletion in SF1 neurons increases body weight and adiposity [13]. However, in contrast with the disruption of the BBSome, loss of the LepR in SF1 neurons did not result in a decrease in energy expenditure under the normal chow condition, although a lower energy expenditure was observed under the high-fat diet condition. In addition, the mice without the LepR in SF1 neurons displayed impaired glucose tolerance, which was not present in the SF1^{Cre}/Bbs1$^{fl/fl}$ mice [30]. Thus, defects in the trafficking of receptors other than the LepRb may contribute to the increase in body weight and adiposity evoked by SF1 neuron BBSome disruption. For instance, loss of the BBSome has been shown to interfere with the brain-derived neurotrophic factor (BDNF)-induced activation of its receptor (TrkB) in cultured human cells [31]. This may affect the activity of SF1 neurons, because of the importance of BDNF-TrkB in modulating the excitability of these neurons [32]. Notably, the BBSome has been involved in the control of many other cellular processes, ranging from gene transcription to development and maintenance of synaptic structures that may contribute to the energy imbalance induced by loss of the *Bbs1* gene in SF1 neurons.

Insulin resistance and elevations in blood pressure and sympathetic nerve discharge, particularly to the kidneys, are hallmarks of obesity and are major risk factors for cardiovascular disease. A notable finding in this study relates to the absence of changes in glucose metabolism, insulin sensitivity, blood pressure, and baroreflex sensitivity in obese SF1^{Cre}/Bbs1$^{fl/fl}$ mice. This phenotype is reminiscent of a subset of obese subjects, referred to as "healthy obese," who do not develop metabolic and cardiovascular diseases [33]. The mechanisms underlying such protection remain elusive. Our findings point to a potential role of the SF1 neuron BBSome in the protection against obesity-related conditions such as diabetes and hypertension. This is further supported by the normal sympathetic nerve traffic to the kidney. Notably, we have previously demonstrated that mice with a similar degree of obesity as the SF1^{Cre}/Bbs1$^{fl/fl}$ mice display an approximate 10–15 mmHg increase in blood pressure associated with elevated baseline renal sympathetic traffic [34,35]. Notably, the vascular-projecting splanchnic sympathetic tone was elevated in SF1^{Cre}/Bbs1$^{fl/fl}$ mice, which might increase blood pressure. This indicates that the increase in splanchnic SNA is not sufficient to trigger blood pressure elevation in the absence of renal and/or lumbar sympathetic nerve activation. Alternatively, splanchnic sympathoexcitation could be due to the stimulation of sympathetic fibers that subserve non-cardiovascular organs. Besides blood vessels, the splanchnic nerve carries fibers that project to many other organs [36]. Irrespective of this phenomenon, the contrasting changes in regional sympathetic activity evoked by loss of the BBSome in SF1 neurons (decreased BAT and WAT SNA vs. increased splanchnic SNA with no change in renal and lumbar SNA) is a strong indication that the SNS is not a monolithic effector activated or inhibited globally in situations requiring physiological adjustments. By contrast, our data support the idea that regional SNA is differentially regulated [34,37]. Additional studies are necessary to understand the mechanisms underlying the differential control of regional SNA in SF1^{Cre}/Bbs1$^{fl/fl}$ mice.

Our study has limitations. First, the absence of hyperphagia in SF1^{Cre}/Bbs1$^{fl/fl}$ mice may be due to the relatively short period of time during which food intake was measured (up to 5 days). A possibility is that measuring feeding behavior for longer periods would reveal differences in food intake. However, the approaches we used to analyze the feeding behavior of SF1^{Cre}/Bbs1$^{fl/fl}$ mice have allowed us to successfully detect differences in food intake in other mouse models [18]. The use of multifiber nerve recording to study the activity of the SNS might not be optimal because of a potential variation in the number of fibers in contact with the recording electrodes, which can influence the outcome of the SNA measurements. However, we used the multifiber recording to study and detect changes in regional sympathetic nerve traffic that were corroborated with other approaches [24,38]. In this study, we detected contrasting changes in sympathetic tone in SF1^{Cre}/Bbs1$^{fl/fl}$ mice, as indicated by the lower BAT and WAT SNA versus higher splanchnic SNA, and the renal and lumbar SNA remained unchanged. Notably, the changes in BAT and WAT SNA were supported by the molecular measurements, validating our method. Nevertheless, single fiber nerve recording could be useful to understand the significance of the elevated splanchnic sympathetic nerve traffic in SF1^{Cre}/Bbs1$^{fl/fl}$ mice.

In conclusion, our data highlighted the essential role of the SF1 neuron BBSome in the control of energy homeostasis. The SF1 neuron BBSome appears to selectively modulate energy expenditure through the SNS activity subserving BAT and WAT. These findings add the BBSome in SF1 neurons to the list of important molecular players that regulate energy balance. Our data also show the requirement of the BBSome in SF1 neurons for obesity-associated conditions such as insulin resistance and hypertension. Because of the difficulty in managing obesity, uncoupling the mechanisms underlying obesity and

its comorbidities highlight the possibility of controlling hypertension and insulin resistance without managing obesity.

FUNDING

This work was supported by funds from the NIH (grants HL084207 to K.R. and J.L.G and HL134850 to J.L.G.), the American Heart Association (18EIA33890055 to J.L.G.) the Department of Veterans Affairs (Merit grant BX004249 to K.R.), and The University of Iowa Fraternal Order of Eagles Diabetes Research Center to K.R. The Zeiss LSM710 in the University of Iowa's Central Microscopy Research Facilities used for confocal imaging is funded by the NIH (grant 1 S10 RR025439-01).

ACKNOWLEDGMENTS

We thank Paul J. Casella for editorial assistance.

CONFLICT OF INTEREST

None declared.

APPENDIX A. SUPPLEMENTARY DATA

Supplementary data to this article can be found online at https://doi.org/10.1016/j.molmet.2021.101211.

REFERENCES

[1] Tirosh, A., Shai, I., Afek, A., Dubnov-Raz, G., Ayalon, N., Gordon, B., et al., 2011. Adolescent BMI trajectory and risk of diabetes versus coronary disease. New England Journal of Medicine 364:1315—1325.

[2] Rahmouni, K., 2014. Obesity-associated hypertension: recent progress in deciphering the pathogenesis. Hypertension 64:215—221.

[3] Cui, H., López, M., Rahmouni, K., 2017. The cellular and molecular bases of leptin and ghrelin resistance in obesity. Nature Reviews Endocrinology 13: 338—351.

[4] Contreras, C., Nogueiras, R., Diéguez, C., Rahmouni, K., López, M., 2017. Traveling from the hypothalamus to the adipose tissue: the thermogenic pathway. Redox Biology 12:854—863.

[5] Kim, K.W., Sohn, J.W., Kohno, D., Xu, Y., Williams, K., Elmquist, J.K., 2011. SF-1 in the ventral medial hypothalamic nucleus: a key regulator of homeostasis. Molecular and Cellular Endocrinology 336:219—223.

[6] King, B.M., 2006. The rise, fall, and resurrection of the ventromedial hypothalamus in the regulation of feeding behavior and body weight. Physiology & Behavior 87:221—244.

[7] Seoane-Collazo, P., Ferno, J., Gonzalez, F., Dieguez, C., Leis, R., Nogueiras, R., et al., 2015. Hypothalamic-autonomic control of energy homeostasis. Endocrine 50:276—291.

[8] Perkins, M.N., Rothwell, N.J., Stock, M.J., Stone, T.W., 1981. Activation of brown adipose tissue thermogenesis by the ventromedial hypothalamus. Nature 289:401—402.

[9] Meek, T.H., Nelson, J.T., Matsen, M.E., Dorfman, M.D., Guyenet, S.J., Damian, V., et al., 2016. Functional identification of a neurocircuit regulating blood glucose. Proceedings of the National Academy of Sciences of the U S A 113:E2073—E2082.

[10] Coutinho, E.A., Okamoto, S., Ishikawa, A.W., Yokota, S., Wada, N., Hirabayashi, T., et al., 2017. Activation of SF1 neurons in the ventromedial hypothalamus by DREADD technology increases insulin sensitivity in peripheral tissues. Diabetes 66:2372—2386.

[11] Lim, K., Barzel, B., Burke, S.L., Armitage, J.A., Head, G.A., 2016. Origin of aberrant blood pressure and sympathetic regulation in diet-induced obesity. Hypertension 68:491—500.

[12] Majdic, G., Young, M., Gomez-Sanchez, E., Anderson, P., Szczepaniak, L.S., Dobbins, R.L., et al., 2002. Knockout mice lacking steroidogenic factor 1 are a novel genetic model of hypothalamic obesity. Endocrinology 143:607—614.

[13] Dhillon, H., Zigman, J.M., Ye, C., Lee, C.E., McGovern, R.A., Tang, V., et al., 2006. Leptin directly activates SF1 neurons in the VMH, and this action by leptin is required for normal body-weight homeostasis. Neuron 49:191—203.

[14] Martínez-Sánchez, N., Seoane-Collazo, P., Contreras, C., Varela, L., Villarroya, J., Rial-Pensado, E., et al., 2017. Hypothalamic AMPK-ER stress-JNK1 Axis mediates the central actions of thyroid hormones on energy balance. Cell Metabolism 26:212—229 e12.

[15] Xu, Y., Hill, J.W., Fukuda, M., Gautron, L., Sohn, J.W., Kim, K.W., et al., 2010. PI3K signaling in the ventromedial hypothalamic nucleus is required for normal energy homeostasis. Cell Metabolism 12:88—95.

[16] Xu, Y., Nedungadi, T.P., Zhu, L., Sobhani, N., Irani, B.G., Davis, K.E., et al., 2011. Distinct hypothalamic neurons mediate estrogenic effects on energy homeostasis and reproduction. Cell Metabolism 14:453—465.

[17] Seoane-Collazo, P., Roa, J., Rial-Pensado, E., Linares-Pose, L., Beiroa, D., Ruiz-Pino, F., et al., 2018. SF1-Specific AMPKalpha1 deletion protects against diet-induced obesity. Diabetes 67:2213—2226.

[18] Guo, D.F., Lin, Z., Wu, Y., Searby, C., Thedens, D.R., Richerson, G.B., et al., 2019. The BBSome in POMC and AgRP neurons is necessary for body weight regulation and sorting of metabolic receptors. Diabetes 68:1591—1603.

[19] Nachury, M.V., Loktev, A.V., Zhang, Q., Westlake, C.J., Peranen, J., Merdes, A., et al., 2007. A core complex of BBS proteins cooperates with the GTPase Rab8 to promote ciliary membrane biogenesis. Cell 129:1201—1213.

[20] Zhang, Q., Yu, D., Seo, S., Stone, E.M., Sheffield, V.C., 2012. Intrinsic protein-protein interaction-mediated and chaperonin-assisted sequential assembly of stable bardet-biedl syndrome protein complex, the BBSome. Journal of Biological Chemistry 287:20625—20635.

[21] Guo, D.F., Rahmouni, K., 2011. Molecular basis of the obesity associated with Bardet-Biedl syndrome. Trends in Endocrinology and Metabolism 22:286—293.

[22] Mujahid, S., Hunt, K.F., Cheah, Y.S., Forsythe, E., Hazlehurst, J.M., Sparks, K., et al., 2018. The endocrine and metabolic characteristics of a large bardet-biedl syndrome clinic population. The Journal of Cinical Endocrinology and Metabolism 103:1834—1841.

[23] Feuillan, P.P., Ng, D., Han, J.C., Sapp, J.C., Wetsch, K., Spaulding, E., et al., 2011. Patients with Bardet-Biedl syndrome have hyperleptinemia suggestive of leptin resistance. The Journal of Cinical Endocrinology and Metabolism 96: E528—E535.

[24] Rahmouni, K., Fath, M.A., Seo, S., Thedens, D.R., Berry, C.J., Weiss, R., et al., 2008. Leptin resistance contributes to obesity and hypertension in mouse models of Bardet-Biedl syndrome. Journal of Clinical Investigation 118:1458—1467.

[25] Starks, R.D., Beyer, A.M., Guo, D.F., Boland, L., Zhang, Q., Sheffield, V.C., et al., 2015. Regulation of insulin receptor trafficking by bardet biedl syndrome proteins. PLoS Genetics 11:e1005311.

[26] Guo, D.F., Cui, H., Zhang, Q., Morgan, D.A., Thedens, D.R., Nishimura, D., et al., 2016. The BBSome controls energy homeostasis by mediating the transport of the leptin receptor to the plasma membrane. PLoS Genetics 12: e1005890.

[27] Seo, S.J., Guo, D.F., Bugge, K., Morgan, D.A., Rahmouni, K., Sheffield, V.C., 2009. Requirement of Bardet-Biedl syndrome proteins for leptin receptor signaling. Human Molecular Genetics 18:1323—1331.

[28] Kim, K.W., Zhao, L., Donato Jr., J., Kohno, D., Xu, Y., Elias, C.F., et al., 2011. Steroidogenic factor 1 directs programs regulating diet-induced thermogenesis and leptin action in the ventral medial hypothalamic nucleus. Proceedings of the National Academy of Sciences of the U S A 108:10673—10678.

[29] Cannon, B., Nedergaard, J., 2011. Nonshivering thermogenesis and its adequate measurement in metabolic studies. Journal of Experimental Biology 214:242—253.

[30] Bingham, N.C., Anderson, K.K., Reuter, A.L., Stallings, N.R., Parker, K.L., 2008. Selective loss of leptin receptors in the ventromedial hypothalamic nucleus results in increased adiposity and a metabolic syndrome. Endocrinology 149(5):2138–2148.

[31] Leitch, C.C., Zaghloul, N.A., 2014. BBS4 is necessary for ciliary localization of TrkB receptor and activation by BDNF. PloS One 9:e98687.

[32] Jo, Y.H., 2012. Endogenous BDNF regulates inhibitory synaptic transmission in the ventromedial nucleus of the hypothalamus. Journal of Neurophysiology 107:42–49.

[33] Stefan, N., Häring, H.U., Hu, F.B., Schulze, M.B., 2013. Metabolically healthy obesity: epidemiology, mechanisms, and clinical implications. The Lancet Diabetes & Endocrinology 1:152–162.

[34] Rahmouni, K., Morgan, D.A., Morgan, G.M., Mark, A.L., Haynes, W.G., 2005. Role of selective leptin resistance in diet-induced obesity hypertension. Diabetes 54:2012–2018.

[35] Guo, D.F., Reho, J.J., Morgan, D.A., Rahmouni, K., 2020. Cardiovascular regulation by the neuronal BBSome. Hypertension 75:1082–1090.

[36] Trudrung, P., Furness, J.B., Pompolo, S., Messenger, J.P., 1994. Locations and chemistries of sympathetic nerve cells that project to the gastrointestinal tract and spleen. Archives of Histology & Cytology 57:139–150.

[37] Morrison, S.F., 2001. Differential control of sympathetic outflow. American Journal of Physiology - Regulatory, Integrative and Comparative Physiology 281:R683–R698.

[38] Zhang, Z., Liu, X., Morgan, D.A., Kuburas, A., Thedens, D.R., Russo, A.F., et al., 2011. Neuronal receptor activity-modifying protein 1 promotes energy expenditure in mice. Diabetes 60:1063–1071.

